# Technical Feasibility of Multimodal Imaging in Neonatal Hypoxic Ischemic Encephalopathy from Ovine Model to Human Case Series

Brian Hagan , Radhika Mujumdar , Jagdish P. Sahoo , Abhijit Das , Anirban Dutta *

Posted Date: 30 May 2023

doi: 10.20944/preprints202305.2080.v1

Keywords: hypoxic-ischemic encephalopathy; electroencephalogram; near-infrared spectroscopy; neurovascular coupling; experimental modal analysis

*Article*

# Technical Feasibility of Multimodal Imaging in Neonatal Hypoxic Ischemic Encephalopathy from Ovine Model to Human Case Series

**Brian Hagan [1], Radhika Mujumdar [1], Jagdish P. Sahoo [2], Abhijit Das [3] and Anirban Dutta [1,*]**

[1] University of Lincoln, Lincoln, UK.
[2] Department of Neonatology, IMS & SUM Hospital, Bhubaneswar, India
[3] The Lancashire teaching Hospitals NHS Foundation Trust, Preston, UK.
* Correspondence: adutta@case.edu

**Abstract:** Hypoxic-ischemic encephalopathy (HIE) secondary to perinatal asphyxia occurs when the brain does not receive enough oxygen and blood. A surrogate marker for 'intact survival' is necessary for the successful management of HIE. The severity of HIE can be classified based on clinical presentation, including presence of seizures, using a clinical classification scale called Sarnat staging; however, Sarnat staging is subjective and the score changes over time. Furthermore, seizures are difficult to detect clinically and are associated with a poor prognosis. Therefore, a tool for continuous monitoring on the cot side is necessary, for example, electroencephalogram (EEG) that non-invasively measures the electrical activity of the brain from the scalp. Then, multimodal brain imaging, when combined with functional near-infrared spectroscopy (fNIRS), can capture the neurovascular coupling (NVC) status. In this study, we first tested the feasibility of a low-cost EEG-fNIRS imaging system to differentiate between normal, hypoxic, and ictal states in a perinatal ovine hypoxia model. Here, the objective was to evaluate a portable cot side device and autoregressive (ARX) modelling to capture the perinatal ovine brain states during a simulated HIE injury. So, ARX parameters were tested with a linear classifier using a single differential channel EEG, with varying states of tissue oxygenation detected using fNIRS, to label simulated HIE states in a perinatal ovine hypoxia model. Then, we showed the technical feasibility of the low-cost EEG-fNIRS device and ARX modeling with support vector machine classification for a human HIE case series with and without sepsis. The classifier trained with the ovine hypoxia data labelled ten severe HIE human cases (with and without sepsis) as "hypoxia" group and the four moderate HIE human cases as the "control" group. Furthermore, we showed the feasibility of experimental modal analysis (EMA) based on the ARX model to investigate the NVC dynamics using EEG-fNIRS joint-imaging data that differentiated six severe HIE human cases without sepsis from four severe HIE human cases with sepsis. In conclusion, our study showed the technical feasibility of EEG-fNIRS imaging, ARX modeling of NVC for HIE classification, and EMA that may provide a biomarker to detect sepsis effects on the NVC in HIE.

**Keywords:** hypoxic-ischemic encephalopathy; electroencephalogram; near-infrared spectroscopy; neurovascular coupling; experimental modal analysis

## 1. Introduction

Hypoxic-ischemic encephalopathy or HIE is one of the most common causes of neonatal death worldwide, accounting for approximately 23 percent of all neonatal deaths (Lawn et al., 2005). Worldwide it is estimated to account for mortality numbers of more than one million annually. HIE also accounts for considerably higher numbers of chronic neurological deficits that create an economic burden, more so in the developing countries. Despite having such an immense societal impact, HIE lacks an adequate rapid diagnostic method (Bryce et al., 2005). In HIE, there is a prolonged lack of oxygen entering the brain; which causes serious neuronal damage within a very

short window of time; approximately two to three minutes if complete lack of oxygen and will lead to a cessation of any neuronal activity shortly thereafter. Due to the direct effect of HIE on the neuronal state, current monitoring and outcome prediction are predominantly based on the electroencephalogram (EEG), which measures neuronal activity in the cerebral cortex. Amplitude-integrated EEG or aEEG has been shown to be an effective prognostic method for long-term neurologic deficits induced by HIE with a ninety percent accurate classification percentage at 6 hours after injury in both positive and negative predictions. Here, positive predictions dictate that a subject will have significant deficits caused by the hypoxic event and negative predictions characterizing recovery of normal neuronal function after the injury. In most studies, the least time to obtain an accepted and accurate prediction of extended deficits was found to be around six hours and the lowest acceptable being three hours where the positive prediction percentages are below 80%, and prior to that time window the method lacks any consistent predictive value (Del Ro et al., 2016),(Toet et al., 1999). Other alternative methods for prognosis in HIE such as magnetic resonance imaging (MRI) have fallen out of favor as they lack prognostic ability or speed in the early stage of brain injury. For example, T1 and T2- weighted MRI take approximately one week for an accurate prognosis resulting from brain swelling from the injury. Also, there is lack of MRI facility in resource poor settings and is often cost prohibitive. According to a meta-analysis done by van Learhoven (Laerhoven et al., 2012), the diagnosis is at best on par with the 6-hour aEEG with a positive predictive score of eighty-three percent and a negative ninety-percent. Then, Chalak et al. (Chalak et al., 2017) presented a neurovascular coupling (NVC)-based approach in HIE using multi-modal imaging with aEEG combined with functional near-infrared spectroscopy (fNIRS) and wavelet coherence analysis. Here, the challenge remains in the continuous monitoring of NVC where Sood et al. (Sood et al., 2016) presented a Kalman Filter based method that allowed online autoregressive (ARX) parameter estimation using time-varying signals and could capture transients in the coupling relationship between EEG and fNIRS signals. Then, the availability of low-cost portable brain imaging devices, e.g., OpenBCI (https://openbci.com/) and M3BA (von Luhmann et al., 2017), can be leveraged for clinical translation of continuous cot-side brain monitoring in limited resource settings that can potentially help for better management of neonates with perinatal asphyxia and improve the long-term neurodevelopmental outcome. In the current study, the overarching objective was to test the feasibility of a low-cost multimodal brain imaging device (von Luhmann et al., 2017) and an ARX-based support vector machine (SVM) classifier for point-of-care HIE monitoring in a limited resource settings.

Continuous monitoring of neurovascular coupling may be superior to clinical scores for HIE classification (Das et al., 2021). The hypoxic state can be rapidly detrimental for the brain neurons due to the large amount of oxygen needed in continuous supply (~10ml/100g tissue/min) and its low reserve, leading to large changes in neuronal firing during oxygen deficits that can affect EEG power spectrum. Indeed, hypoxia effects on the EEG power spectrum have been extensively studied in both humans and in animal models (Choi, 1990),(Walsh et al., 2011). The spectral density, more commonly referred to as the power spectrum of the signal, makes the EEG signal easier to analyze based on rhythms which can be monitored over time as a spectrogram. The effect of hypoxia on the power spectrum has been studied using animal models (Kyng et al., 2015), e.g., Goel and colleagues (Goel et al., 1996) in an animal model of a neonatal piglet showed results from hypobaric hypoxia that was induced for 30 minutes using 10% oxygen concentration in air. Then, the airway was occluded for seven minutes, during which the piglet's neural firing ceased, and then the piglet was resuscitated afterwards. Throughout the protocol, the EEG was monitored while the piglet was anesthetized. At the end of both segments, airway occlusion and resuscitation, the power spectrum was calculated, and one remarkable feature was the spectral dispersion where the low-frequency alpha and theta firings were most affected by the hypoxia; and there was a degree of disproportionality in the recovery of power of the 3 dominant frequency bands (1.0-5.5 Hz, 9.0-14.0 Hz, and 18.0-21.0 Hz) relative to their mean recovered power. Time domain features have also been used such as Hjorth parameters. The Hjorth parameters are simple statistical calculations on the EEG signal, with the first parameter known as the activity of the signal which is the variance of the amplitude for a window of

 doi:10.20944/preprints202305.2080.v1



the signal in time and the second Hjorth parameter known as the mobility of the signal. Mobility is defined as the square root of the ratio of the first parameter of the rate of change of the signal, divided by the actual first parameter of the signal or the rate of change of the activity divided by the activity of the signal. The last of the Hjorth parameters is known as the complexity of the signal, which is the second derivative of the activity divided by the first derivative of the activity. Each of these Hjorth parameters changed during HIE and were found useful especially in the classification of early partial seizure onset (Jouny and Bergey, 2012). Then, aEEG is a major clinical tool for long-term prognosis of HIE; however, it uses ten-minute windows for calculation and needs at least 6 hours of data for accurate prognosis. Here, aEEG on its own needs prolonged data acquisition for accurate prognosis that may outrun the early treatment window for HIE. Also, aEEG can be processed using Washington University-Neonatal EEG Analysis Toolbox (WU-NEAT) to estimate neurovascular coupling (NVC) in conjunction with functional near-infrared spectroscopy (fNIRS)(Das et al., 2021) which can be used for HIE classification (Chalak et al., 2017). Another time series analysis is autoregressive (AR) modelling that takes a segment of data and fits to the current data point a linear combination of previous data points multiplied by parameters that have a fixed value throughout the segment. The AR model requires matrix calculations to acquire these parameter values and requires validation to ensure that it is adequately capturing the EEG signal properties and not the noise especially when detecting seizure activity (Greene et al., 2008). If the AR model adequately fits the data, the power spectrum trends are captured in the transfer function output of the system model and can be reconstructed. Then, operational modal analysis using AR with eXogenous input (ARX) model can provide mechanistic insights from the NVC system model with the simultaneously acquired EEG-fNIRS data. We have extended published algorithms for online multimodal brain imaging using EEG and fNIRS in our prior work (Sood et al., 2016).

The current study is motivated by recent findings on the role of NVC in the prediction of brain abnormalities in neonatal encephalopathy (Das et al., 2021). Das et al. (Das et al., 2021) found NVC to be a promising biomarker in neonatal HIE that was superior to the total Sarnat score (Mrelashvili et al., 2020) for the prediction of abnormal brain MRI in the later stages. In estimating coherence, stationarity and ergodicity of the signal is assumed, which needs preprocessing of the raw EEG data to remove trends and low-frequency variations. Then, the modelling accuracy becomes more challenging when the spectra contain sharp peaks, e.g., during rhythmic activity (Faes et al., 2004). Therefore, an ictal classifier based on EEG spectral features was developed using the Children's Hospital of Boston and the Massachusetts Institute of Technology (CHB-MIT) dataset (Goldberger et al., 2000) to separately label seizure activity (Shoeb and Guttag, 2010). Then, support vector machine (SVM) was used with the AR parameters to classify EEG (Ahmed et al., 2016) into various experimentally induced states in an ovine model of perinatal asphyxial arrest (Vali et al., 2019). Here, we applied AR modelling and assumed AR parameters being constant throughout the selected window size (Al-Fahoum and Al-Fraihat, 2014). Ahmed and colleagues (Ahmed et al., 2016) have used a multiclass SVM classifier for the best estimation of an outcome based on a commonly used clinical grade of one to four; a grade of one being non- to mild- abnormalities, two being moderate, three being major EEG depression, and four being a severe EEG discontinuity. Their classifier overall had an eighty-seven percent accuracy in classifying the recovery grade of newborns from HIE, and was found to be one of the most effective such classifiers while others being as accurate as seventy-seven percent (Stevenson et al., 2013). Here, we also performed ARX modeling using EEG-fNIRS data from the ovine model of perinatal asphyxial arrest (Vali et al., 2019). The objective was to test the feasibility of a low-cost EEG-fNIRS device and the ARX based linear classifier to label simulated HIE states in a perinatal ovine hypoxia model. Then, we applied the ARX based linear classifier trained with perinatal ovine hypoxia model data to a human case series on perinatal HIE with and without sepsis. We also investigated experimental modal analysis (EMA) of the NVC system model that provided mechanistic insights from simultaneously acquired EEG-fNIRS data. Here, the ARX model allowed estimation of the modal parameters and frequency response functions (FRF) of the NVC system. Then, the FRF of the EEG power as input and the hemodynamic (fNIRS) changes as output

Preprints (www.preprints.org) | NOT PEER-REVIEWED | Posted: 30 May 2023 doi:10.20944/preprints202305.2080.v1



were used for the EMA of the NVC system dynamics for the mechanistic insights in to the HIE (with versus without sepsis).

## 2. Materials and Methods

### *2.1. Animal Model and Data Processing*

The preparation of ovine subjects was carried out in accordance with the Institutional Animal Care and Use Committee at the State University of New York at Buffalo, USA (Hagan, 2018), (Vali et al., 2017),(Vali et al., 2018). Term (140-147 days) pregnant ewes were obtained from New Pasteur Family Farms (Attica, NY). After an overnight fast, the pregnant ewe was anaesthetised with intravenous diazepam and ketamine. The ewe was continuously monitored using a pulse oximeter and an end-tidal carbon dioxide monitor. The ewe was intubated with a 10mm cuffed endotracheal tube and ventilated with 21% oxygen and 2-3% isoflurane at a breathing rate of 16 breaths per minute. The perinatal ovines were delivered by caesarian section and partially exteriorized and intubated. Once the delivery process was completed, excess fluid that remained in the lungs of the newborn was removed via passive measures, by tilting of the head back and forth simulating the process by which fluid is removed during birth. Once the excess liquid was removed, the airway was occluded to prevent gas exchange. The catheters were then placed in the jugular vein and right carotid artery to sample blood and administer any necessary medication. A two-millimeter flow probe (Transonic Systems Inc, Ithaca, NY) was placed around the left carotid artery and a four-millimeter flow probe was placed in the left pulmonary artery. The electrocardiogram electrodes were then placed in the right and left axilla and right inguinal area, a standard three-lead setup. The ECG100C (Biopac. Inc.) was used with Acknowledge software to record data from leads I, II and III of the ECG. The saturation of preductal arterial oxygenated hemoglobin was monitored by a pulse oximeter placed on the right forelimb of the neonate. The low-cost wireless EEG-fNIRS (750nm and 850nm) sensors (OEM from Technische Universität Berlin)(von Luhmann et al., 2017) were placed on the forehead for continuous measurement at 500 Hz for EEG and 10 Hz for fNIRS (see Figure 1). Our low-cost wireless EEG-fNIRS (750nm and 850nm) sensors (Bionics Institute, Australia) were validated using off-the-shelf EEG (Biopac Inc., USA) and fNIRS (Nonin Medical, USA) sensor data from the established perinatal asphyxiated lamb model experiments – see the experimental protocol by Vali et al. (Vali et al., 2018).

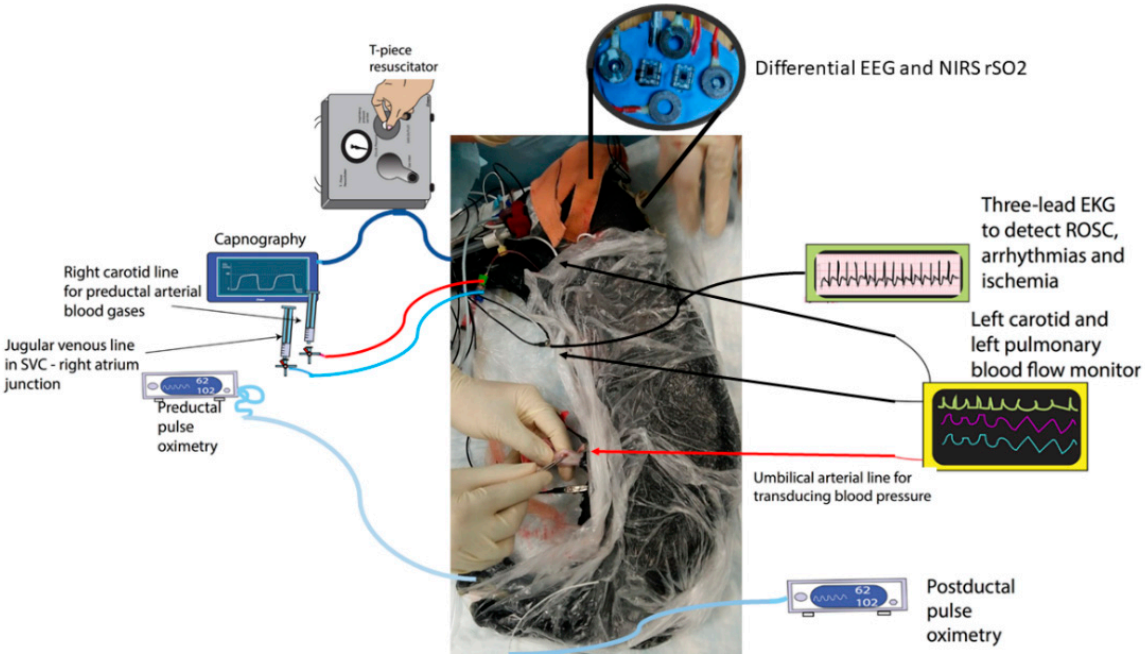


**Figure 1.** Differential EEG and the fNIRS sensors were added to the perinatal asphyxiated lamb model experiments (Vali et al., 2018). Figure was adapted from Figure 1 of Vali et al., 2017.

Preprints (www.preprints.org) | NOT PEER-REVIEWED | Posted: 30 May 2023 doi:10.20944/preprints202305.2080.v1



Following instrumentation, the umbilical cord was occluded until asystole, which is defined as the complete lack of carotid artery flow, arterial blood pressure, and heart rate. The lamb remained in the asystole for five minutes, and then resuscitation was started. Positive pressure ventilation (PPV) via an endotracheal tube was provided with 20% oxygen and was performed using a T piece at a rate of 40 breaths per minute (Vali et al., 2017). After a minute of ventilation, chest compressions were initiated and coordinated with chest compressions (CC) in the ratio of 3:1 (3 CC: 1 PPV). After 5 minutes of resuscitation, if the lambs did not have spontaneous return of circulation (ROSC – defined as heart rate >60/m with systolic blood pressures >30 mmHg), medications (epinephrine or vasopressin) were administered through an umbilical venous catheter. Blood gases were obtained at intervals and the lambs were ventilated after ROSC for 2-3 hours. If the lambs had ROSC, resuscitation was stopped at 20 minutes. Data from five ovine subjects were analysed in this study with a gestational time of 139-142 days, as shown in Table 1. The data analysis followed five major portions: Raw Data Extraction, Preprocessing, Autoregressive Modelling, Classification, and Validation. The workflow presented in Figure 2 was used to obtain results from the EEG and fNIRS systems starting with the extraction of raw data.

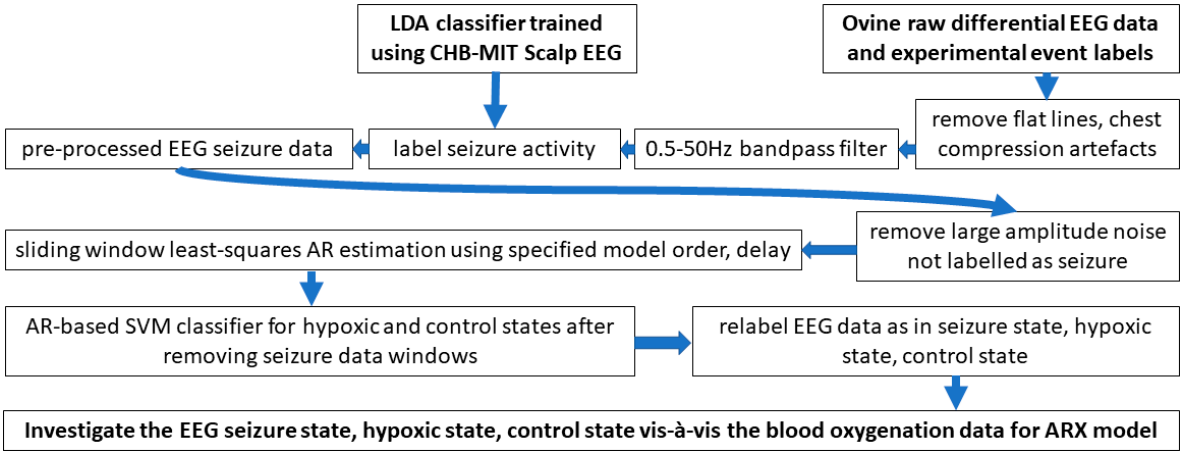


**Figure 2.** Algorithmic workflow for processing perinatal ovine EEG data.

The major events were labelled offline as follows. Start of EEG, or the start of our experiment; then neonate delivery after which the asphyxiation of the subject. Here, from the beginning of EEG to the start of asphyxiation, the data was labelled as control or normal. The next major event was the point of no cardiovascular function, known as asystole. Data between the time of neonate delivery and asystole was labelled as ischemic data. The next event was the start of resuscitation. The data between asystole and the start of resuscitation were labelled the asystole segment. The two portions consisting of ischemic and asystole data segments were combined into a more generalized hypoxia phase for our AR-SVM classifier testing. The last event was the recovery of spontaneous circulation or ROSC. So, the data segment between the start of resuscitation and the ROSC was labelled as the chest compression segment, and then, the last segment was the recovery segment in the case of ROSC of the subject.

Data preprocessing – removal of chest compression: As EEG is affected by the movement artefacts due to chest compressions so that data segment was completely removed during preprocessing.

Data preprocessing – removal of flat lines: The next stage of the preprocessing was to remove sections of the data where electrode contact was lost or obstructed which can show as a flat-line artefact in the EEG. The EEG flat lines were removed by measuring the standard deviation of the signal in the sliding window after visual confirmation.

Data preprocessing – correcting for baseline drift: The removal of the baseline drift is the next step in the preprocessing pipeline. EEG is considered a zero mean signal so if the signal mean is not zero over time, then it was considered as baseline drift artefact. In the case of baseline drift artefact,

Preprints (www.preprints.org) | NOT PEER-REVIEWED | Posted: 30 May 2023 doi:10.20944/preprints202305.2080.v1



the EEG data was adjusted back to a zero-mean using the 'detrend' function in Matlab (Mathworks, Inc.).

Data preprocessing - bandpass filtering of data: A bandpass filter was designed with cutoff frequencies that were set to 0.5 to 50 Hz (neonates rarely have high gamma activity (Takeuchi et al., 2021)) thereby removing both low-frequency artifacts (common causes of non-stationarity) and high-frequency noise. We applied a fifth-order filter that provided a stable filter for our specific cut-off frequencies using the 'butter' function in Matlab (Mathworks, Inc.).

**Table 1.** Five full-term ovine subjects used in the animal study.

| Subjects | Gestational Time (Days) | Weight (lbs) | Sex |
|---|---|---|---|
| 11/16-1 | 142 | 5.5 | Male |
| 12/13 | 141 | 3.05 | Female |
| 3/26 | 139 | 4 | Male |
| 11/16-2 | 142 | 5.5 | Male |
| 11/15 | 141 | 4.4 | Male |

Data preprocessing – LDA binary classifier for seizure: The next stage of the preprocessing pipeline was to label ictal activity using a sliding window of the data (Al-Fahoum and Al-Fraihat, 2014) as seizure activity occurred frequently and we aimed at hypoxia classification using background (non-seizure) EEG activity (Staba and Worrell, 2014). LDA classifier training was using the Children's Hospital of Boston and the Massachusetts Institute of Technology (CHB-MIT) dataset (Goldberger et al., 2000). CHB-MIT scalp EEG dataset contains 22 subjects from children who have been removed from antiepileptic medication and suffered seizures. The sampling rate for all data was 256Hz, and the international 10-20 standard montage was used for recording. A physician trained in EEG-based seizure detection manually labelled the occurrence of ictal activity in the CHB-MIT dataset. To maximize the scalability of the LDA classifier from CHB-MIT dataset to our EEG measurement, only one channel of differential data was chosen for training the classifier, as described next.

The differential EEG channel used in our perinatal ovine study was comparable to the Fz-Cz electrode pair from the human 10-20 labels. Therefore, Fz-Cz electrode data was processed for differential EEG like our perinatal ovine data but we did not use their (Shoeb and Guttag, 2010) SVM classifier that had several hyperparameters. We used simpler linear discriminant classifier (LDA) that was trained using the labelled CHB-MIT dataset (using 3.4 s sliding window which was longer than 2 s used in their SVM classifier (Shoeb and Guttag, 2010)). Our chosen features were alpha and low gamma bandpower (Louis et al., 2016). Here, LDA is a binary classifier that generates a linear decision plane to maximize the accuracy of binary classification. To avoid overfitting, a five-fold cross-validation was used, which divided the EEG data into five segments and used four-fifth of the data to train the classifier and one-fifth to test and did this processing five different times so all the EEG data can be used for both testing and training. This method is widely used in machine learning to avoid generating over-fit classifiers. Once the LDA classifier was trained by the labelled CHB-MIT dataset, the Fz-Cz EEG ovine data in 2 s sliding window was run through the binary classifier, and the windows with seizure were labelled.

Data preprocessing – removal of large-amplitude data segments: The last in the preprocessing was to remove data segments containing large activity (and not labelled as seizure); this was done by finding the overall standard deviation of the EEG data and removing data segments that had mean larger than two standard deviations of the whole EEG data.

Autoregressive (AR) modelling of the EEG data: AR model is a linear model that fits the current output using a defined number of previous outputs, multiplied by the same number of coefficients, known as AR parameters. The AR parameters are optimized based on the linear algebra principle of least-squared estimate for the best fit where AR model yields higher resolution for spectral analysis than nonparametric approaches when the signal length is short. If an accurate AR model is

constructed, then the spectral analysis of the signal can be solely described and reconstructed from AR parameters. Then, AR model delay was included in our model and the delay calculation was done using autocorrelation, which is a measure of mutual information shared between the signal and a time-shifted version of itself. The analysis of the autocorrelation of the data was performed for every possible positive delay. The maximum value denotes the time point when there is the most shared information. The delay was calculated for each ovine subject separately from the control phase of the EEG data. The AR model order is the other property of the model that must be optimized, which was done to make sure that the system is being accurately modelled while also being least computationally expensive, e.g., using Akaike's information criterion (AIC). Prior work (Goel et al., 1996) also found an optimal AR model order of six for a similar kind of EEG data. After AR modelling the EEG data, these AR parameters were plotted in 3D to visualize clusters from the non-ictal background EEG activity. The ictal activity was labelled using a first level LDA classifier – see section *Pre-processing - Seizure Binary Classifier*. Then, AR parameters were used as features to visualize the clusters for all the three different experimental conditions in the 3D AR feature space; seizure state, hypoxia state, normal/control state.

Support vector machine (SVM) classification using EEG AR parameters: Separation into the three experimentally induced states, normal/control, hypoxia, and seizure, was done using two different linear classifiers in the hierarchy. The first of the two linear classifiers in the hierarchy were the LDA seizure classifier that was trained using the CHB-MIT dataset – see section *Pre-processing - Seizure Binary Classifier*. This binary classifier was applied to identify the data segments that contained ictal activity which were removed before training and testing the second level SVM classifier using the background EEG (3.4-second sliding window). The second level SVM classifier was used to classify the AR parameters from the seizure-free (background) EEG data segments into the hypoxia state and the control (normal) state. Here, AR parameters were used as features (see Supplementary Materials, Figures S1 to S3), and the response variable used for training and validation were the event markers from the animal experiment. SVM classifier was chosen for a more generalizable decision plane since this SVM classifier that was trained using perinatal ovine data was then applied to human perinatal case series. To avoid overfitting the SVM classifier, a five-fold cross-validation was used.

Support vector machine (SVM) classification using EEG-fNIRS ARX Parameters: We applied the ARX model to the EEG-fNIRS data (here, 60-second sliding window used due to slower fNIRS signal) for the second level SVM classifier using seizure-free data segments for labeling hypoxia and control (normal) states. We used basic nirs-toolbox (Santosa et al., 2018) script in Matlab (Mathworks, Inc.) to process the fNIRS data (750nm and 850nm). Specifically, we used the following modules with default parameters; nirs.modules.OpticalDensity, nirs.modules.BeerLambertLaw, and nirs.modules.AR_IRLS. We used AR-IRLS model (Huppert, 2016) that used both prewhitening and robust regression to remove noise from the data. ARX model order of six from AIC was comparable to our previous work (Sood et al., 2016) that used fNIRS oxy-hemoglobin signal in the low frequency (0.1 Hz) range as the output and the transformed EEG bandpower as the input (Sood et al., 2016). In this study, we used an EEG frequency band of 1.0-21.0 Hz due to the dominant frequencies found in a related prior work (Goel et al., 1996). Then, the ARX parameters ('arx' in MATLAB) were used as features in the SVM classifier, and the response variable used were the event markers from our animal experiment. To avoid overfitting the classifier, a five-fold cross-validation was used.

Hierarchical classifier outcome vis-a-vis carotid flow: After the hierarchical classifier was found from the perinatal ovine data, the classifier outcome was compared with the carotid blood flow data. Here, the objective was to compare with the changes in the carotid flow rate (irrespective of the manually placed event boundaries) when the ovine subject physiologically entered the global hypoxia stage.

### *2.2. Human Data Acquisition and Feasibility Testing*

Human perinatal study was conducted based on convenience sampling at the Department of Neonatology and approved by the Institutional Review Board (IRB) of the IMS & SUM hospital, Bhubaneswar, India. The study objectives were to test the feasibility of the EEG-fNIRS joint imaging

 doi:10.20944/preprints202305.2080.v1



for the ARX-based SVM classifier that was trained with the perinatal ovine data to detect the severity of human perinatal HIE. The study was a prospective observational study. Ten newborns with moderate to severe HIE and four severe HIE cases with sepsis were recruited for the feasibility study. Sepsis screening was performed according to the clinical guidelines at the IMS & SUM hospital, Bhubaneswar, India. Specifically, sepsis was suspected when there was a history of lethargy, poor feeding, fever or hypothermia or temperature instability, abdominal distension, feeding intolerance, tachypnea. The suspicion was corroborated with positive sepsis screen (total leukocyte count <5000/cmm or absolute neutrophils count < 1800/cmm, micro ESR > 15mm in the first hour, immature to total neutrophil ratio > 0.2, CRP > 10mg/dl, any 2 of the 4 parameters positive meant sepsis screen positive). Sepsis was also confirmed if the blood culture was positive. Here, the physical and the neurological examination was performed by neonatologists trained with Sarnat and Sarnat scoring criteria (Sarnat and Sarnat, 1976).

The inclusion and exclusion criteria were:

- Inclusion criteria: Neonates with gestation > 35wks and >1800gm admitted to the neonatal intensive care unit (NICU) for the treatment of perinatal asphyxia.
- Exclusion criteria: Premature babies < 35wks, Babies with multiple congenital anomalies, Not giving consent for inclusion in the study.

The experimental setup is shown in Figure 3 where the parietal EEG channels were averaged and subtracted from the averaged frontal channels to get a single channel EEG data. The bilateral frontal-parietal fNIRS channels were also averaged to get a single channel of fNIRS data. The preprocessing used in the perinatal ovine model study was applied to the human EEG-fNIRS data. The first level LDA classifier (trained using human perinatal EEG data from the CHB-MIT dataset (Shoeb and Guttag, 2010) – see section *Pre-processing - Seizure Binary Classifier*) was applied to label the seizure segments in the EEG data. Then, the second level SVM classifier in the hierarchical classifier, trained using the ovine EEG-fNIRS data, was applied to 60 sec sliding windows of the human EEG-fNIRS data to label the hypoxia and the control (normal) states. Then, for mechanistic investigation of the NVC system using modal analysis (Arora and Dutta, 2022), we applied EMA using the ARX system model ('arx', System Identification Toolbox). Here, we performed EMA of the estimated NVC system that was estimated from the EEG-fNIRS data. Input and output time series were stored using a data object in the time domain ("iddata" in Matlab). We used the modal analysis functions 'modalfrf' to determine the frequency response functions (FRF), 'modalfit' to determine the modal parameters of the FRF, and 'modalsd' to generate a stabilization diagram for the modal analysis in Matlab (Mathworks, Inc.). A single set of modal parameters was generated using the least squares complex exponential (LSCE) algorithm in Matlab (Mathworks, Inc.) by analyzing multiple response signals simultaneously in 'modalsd'. Then, a stabilization diagram was used to identify the physical modes by examining the stability of the poles as the number of modes increased. Here, the given pole was considered stable in frequency if its natural frequency changes by less than 1% and stable in damping if the damping ratio changes by less than 2% as the model order increases in the stabilization diagram.

Preprints (www.preprints.org) | NOT PEER-REVIEWED | Posted: 30 May 2023 doi:10.20944/preprints202305.2080.v1




**Figure 3.** Experimental setup for perinatal human study in the NICU using the low-cost EEG-fNIRS device (OEM from Technische Universität Berlin) – see the bottom left inset. The 8 EEG electrodes were distributed bilaterally in the frontal and the parietal areas – see the top right inset. The two fNIRS sources were placed bilaterally in the frontal area while the two fNIRS detectors were placed bilaterally in the parietal area in the cap (using black cloth head band).

## 3. Results

### *3.1. Results from Perinatal Ovine Study - Classification Based on Autoregressive Parameters*

Clustering of the AR parameters for the experimentally induced HIE states in the ovine model (see upper panel of Figure 4) allowed binary decision planes for the first level (seizure vs. non-seizure EEG data) and the second level (hypoxia vs. control EEG data) in the hierarchical linear classifier using a sliding window of 3.4 seconds for the EEG data. Here, the sliding window of 3.4 seconds (longer than 2 s used in the prior work with SVM classifier (Shoeb and Guttag, 2010)) was found to be adequate for the estimation of AR parameters for the reconstruction of the EEG power spectrum (Al-Fahoum and Al-Fraihat, 2014) – more details in the thesis (Hagan, 2018). The first level of the hierarchical linear classifier determined the seizure state using LDA classifier applied on EEG data in sliding windows of 3.4 seconds where the confusion matrix of the binary classifier trained with the human CHB-MIT dataset is shown in Table 2. Here, the accuracy is 92.68%, sensitivity is 76.88%, and specificity is 93% which is comparable to the prior work (Shoeb and Guttag, 2010). Then, the decision plane of the LDA seizure classifier was used to identify and label the seizure data segments (= 3.4 sec) in the perinatal ovine EEG data. Then, the second level classifier was trained to separate the control (normal) segment from the hypoxia segment using either the AR parameters from EEG data (with 3.4 sec sliding window) or the ARX parameters from the EEG-fNIRS (with 60 sec sliding window). AR parameters performed moderately well to separate the control (normal) segment from the hypoxia segment (see Table 3) where the accuracy was 98.44%, sensitivity was 70.75%, and specificity was 81.78%. However, with ARX parameters from EEG-fNIRS data, the classifier performance to separate the control (normal) segment from the hypoxia segment (see Table 4) (also Supplementary Materials, Figures S1 to S3) improved sensitivity and specificity with the accuracy at 95.30%, sensitivity at 91.95%, and specificity at 96.75%. Figure 4 shows an illustrative example of the correspondence of the classification of the control (normal) segment from the hypoxia segment vis-à-vis normalized carotid flow recordings and global hypoxia (oxygen influx based on oxygen saturation).

Preprints (www.preprints.org) | NOT PEER-REVIEWED | Posted: 30 May 2023 doi:10.20944/preprints202305.2080.v1



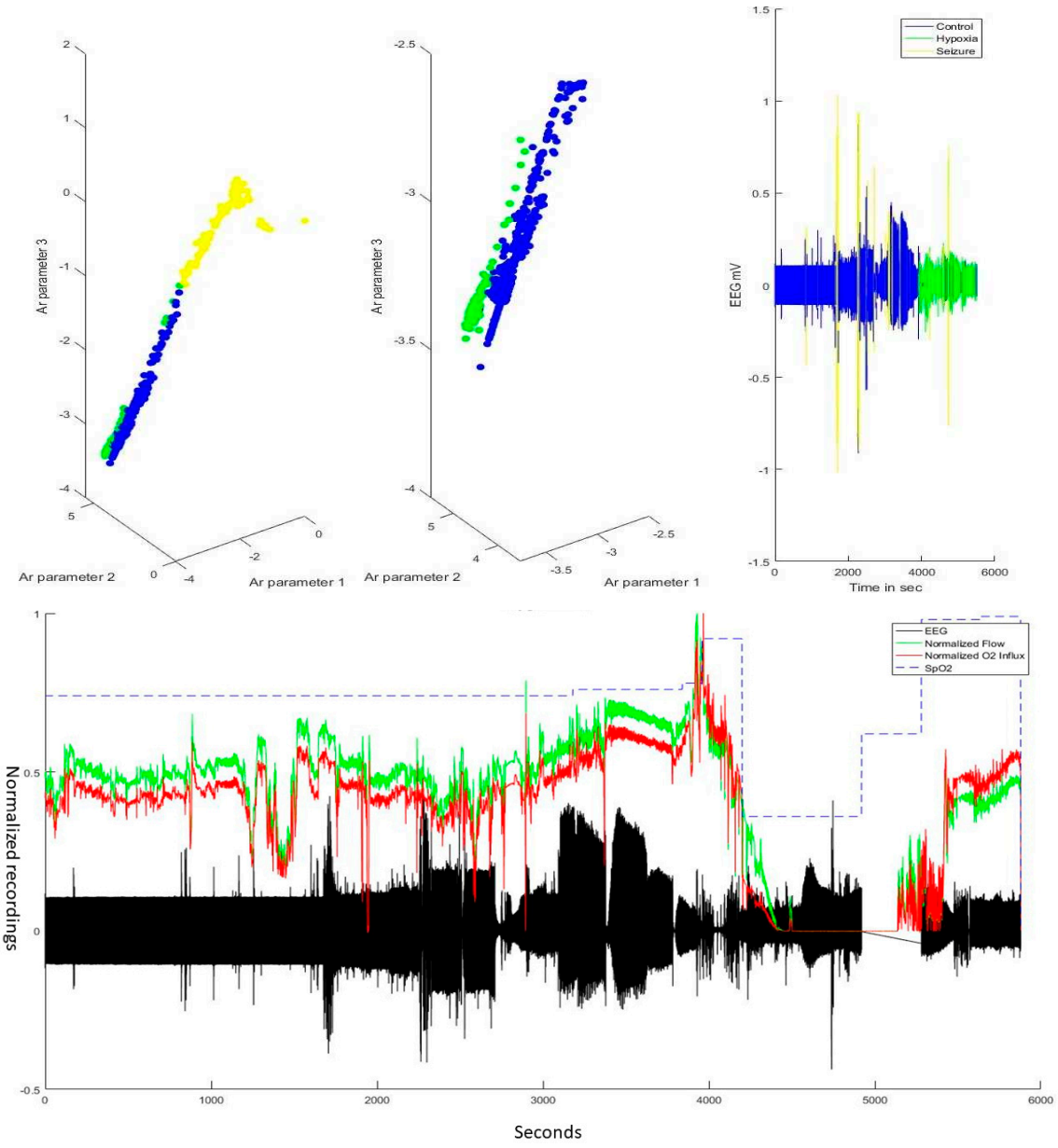


**Figure 4.** An illustrative example of subject 11/16-1 – comparing EEG classifier labels vis-à-vis carotid blood flow and oxygen influx data. Top panel shows the labeling by the hierarchical classifier in the AR feature space that could discriminate the brain state – control or normal (blue), hypoxia (green), seizure (yellow). Bottom panel shows the corresponding carotid flow and oxygen (O2) influx from the oxygen saturation (SpO2) data. Note that around 4000 seconds timepoint, the carotid blood flow increase is followed by a steep decrease – the response of the neonate to asphyxial arrest (Vali et al., 2019). The chest compression and resuscitation data sections were removed (around 5000 seconds) that was followed by ROSC with the return of the carotid flow and oxygen influx. Here, the gap in the EEG data (in black) before ROSC and after asphyxial arrest is due to the removal of the artefactual (due to chest compression) EEG data.

Preprints (www.preprints.org) | NOT PEER-REVIEWED | Posted: 30 May 2023 doi:10.20944/preprints202305.2080.v1



**Table 2.** Confusion matrix of the ictal state classification using the LDA classifier.

| | | Predicted Class | |
|---|---|---|---|
| N = | 8670 | P | N |
| Actual Class | P | 143 | 43 |
| | N | 592 | 7892 |

**Table 3.** Confusion matrix of the hypoxia classification based on AR parameters from EEG using the SVM classifier.

| | | Predicted Class | |
|---|---|---|---|
| N = | 8484 | P | N |
| Actual Class | P | 1819 | 752 |
| | N | 1077 | 4836 |

**Table 4.** Confusion matrix of the hypoxia classification based on ARX parameters from EEG-fNIRS using the SVM classifier.

| | | Predicted Class | |
|---|---|---|---|
| N = | 8484 | P | N |
| Actual Class | P | 2364 | 207 |
| | N | 192 | 5721 |

*3.2. Results from the human feasibility study*

A non-technical staff was trained to conduct cot-side continuous EEG-fNIRS data acquisition in NICU that was established in a limited resource setting with one day of shadowing of a technical expert to learn the experimental protocol – setup shown in the Figure 3. The two-level hierarchical classifier developed using the ovine EEG-fNIRS data (see Figure 4) was applied to the human EEG-fNIRS data. The hierarchical classifier labelled the six severe HIE cases and four severe HIE cases with sepsis as "hypoxia" and the four moderate HIE cases as the "control" – hypoxia and control labels are based on the perinatal ovine experiment (see Figure 4). Here, EMA provided insights into the NVC modes (Arora and Dutta, 2022) where the severe HIE and the severe HIE with sepsis cases were found to be different in the stabilization diagram.

*3.3. Results from the EMA of the human NVC*

Figure 5 shows the stabilization diagrams of the NVC system estimated from the EEG-fNIRS signals (60 s sliding window) from six severe HIE human perinatal cases, four severe HIE human perinatal cases with sepsis, and four moderate HIE human perinatal cases. Here, the stabilization diagrams of the four moderate HIE human perinatal cases did not show a dip around 1Hz in the averaged frequency response function. Also, the four severe HIE human perinatal cases with sepsis had a dip around 1 Hz as well as a stable pole mainly in the frequency between 0.5Hz and 1Hz.

Preprints (www.preprints.org) | NOT PEER-REVIEWED | Posted: 30 May 2023 doi:10.20944/preprints202305.2080.v1



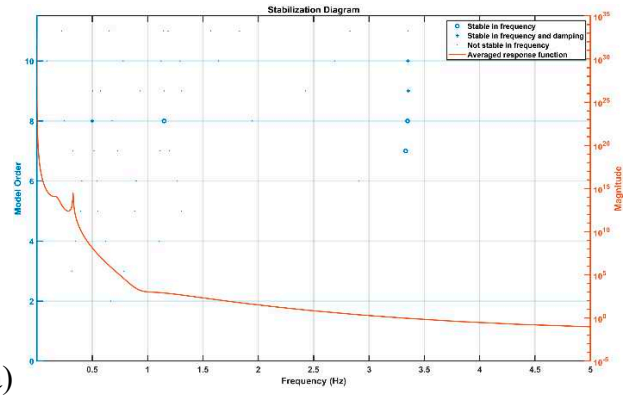


(a)

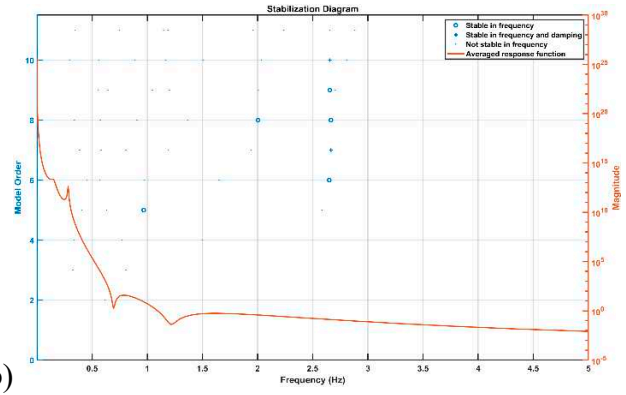


(b)

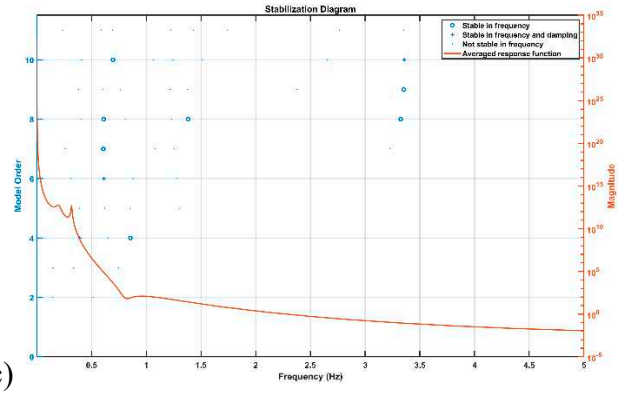


(c)

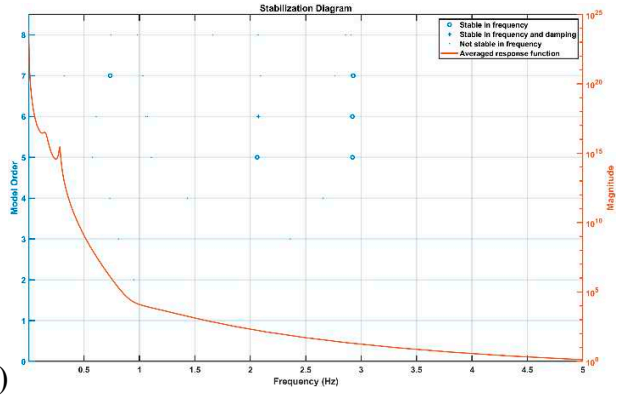


(d)

Preprints (www.preprints.org) | NOT PEER-REVIEWED | Posted: 30 May 2023 doi:10.20944/preprints202305.2080.v1



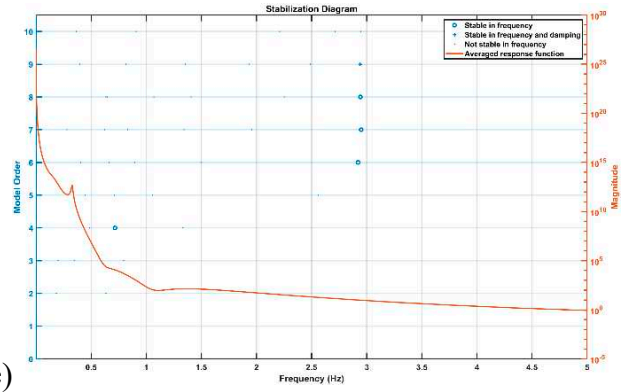


(e)

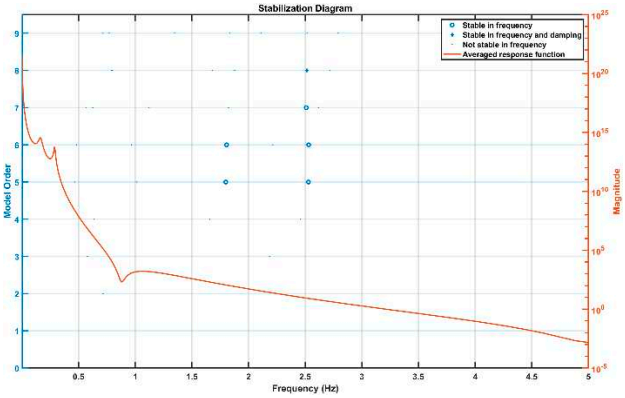


(f)

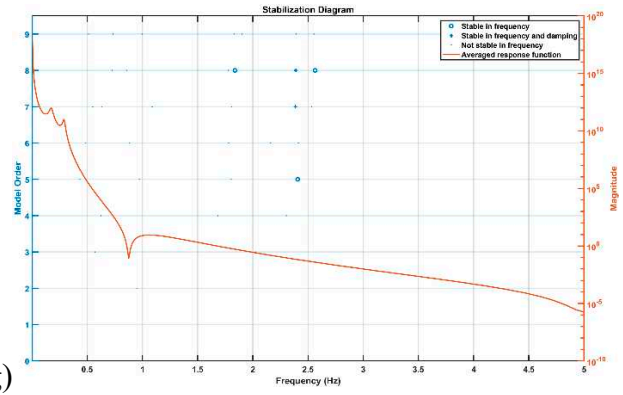


(g)

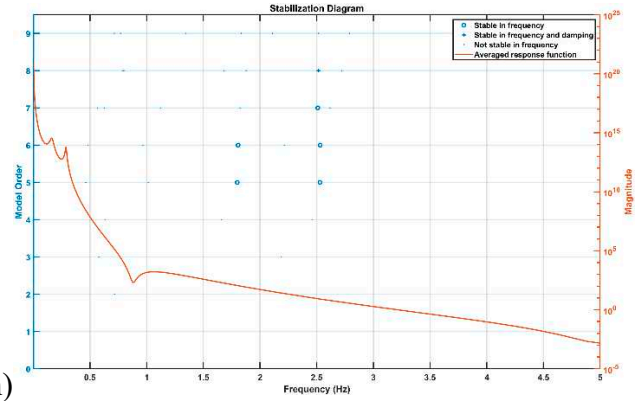


(h)

Preprints (www.preprints.org) | NOT PEER-REVIEWED | Posted: 30 May 2023 doi:10.20944/preprints202305.2080.v1



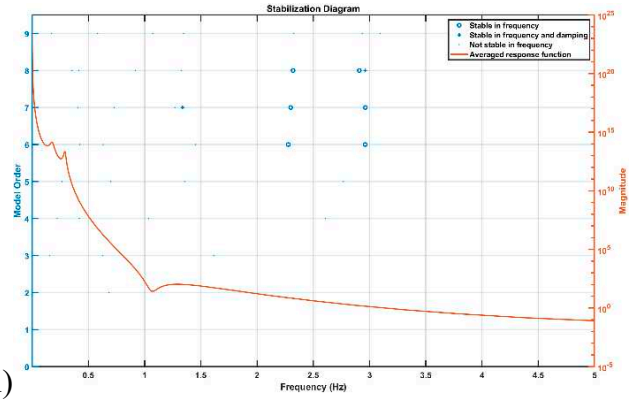


(i)

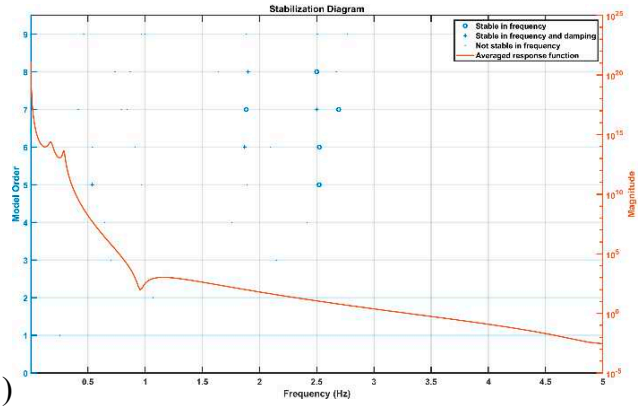


(j)

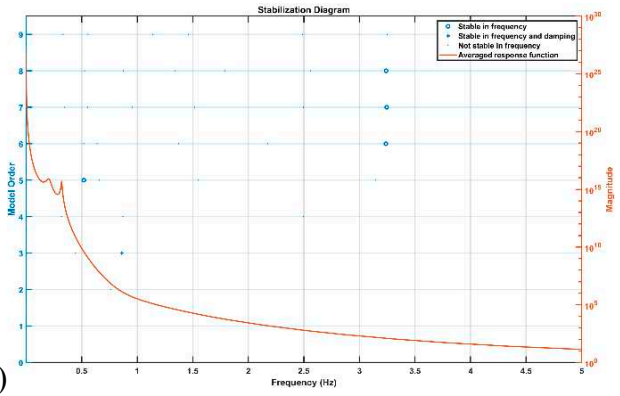


(k)

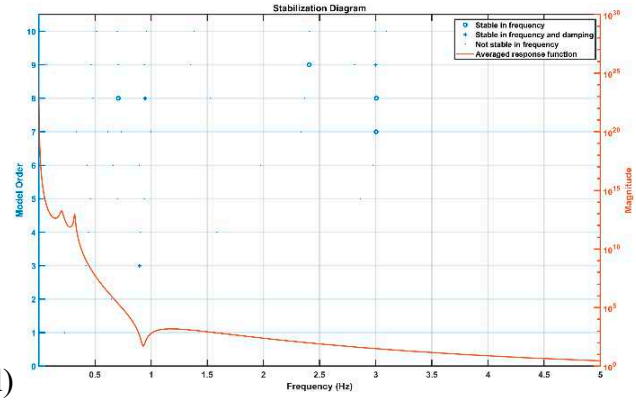


(l)

Preprints (www.preprints.org) | NOT PEER-REVIEWED | Posted: 30 May 2023 doi:10.20944/preprints202305.2080.v1



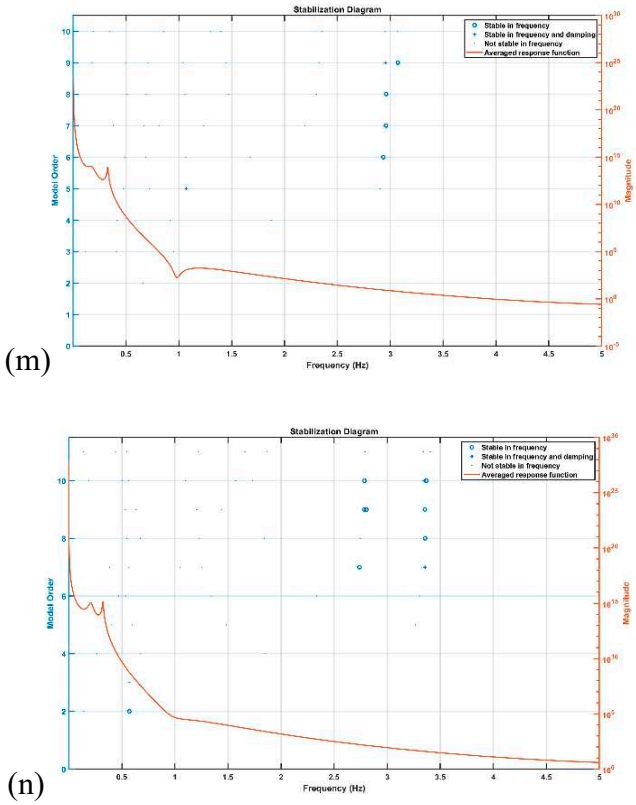


**Figure 5.** Stabilization diagram of the ARX model of the neurovascular coupling system. (a) subj 1: moderate HIE, (b) subj 2: severe HIE with sepsis, (c) subj 3: severe HIE with sepsis, (d) subj 4: moderate HIE, (e) subj 5: severe HIE with sepsis, (f) subj 6: severe HIE, (g) subj 7: severe HIE, (h) subj 8: severe HIE, (i) subj 9: severe HIE, (j) subj 10: severe HIE, (k) subj 11: moderate HIE, (l) subj 12: severe HIE with sepsis, (m) subj 13: severe HIE, (n) subj 14: moderate HIE.

## 4. Discussion

Our study showed the feasibility of training a SVM classifier with the ARX parameters from the perinatal ovine model EEG-fNIRS data and then applying the SVM classifier to the human data to detect HIE severity. The SVM classifier was at the second level of our hierarchical classifier where the first level was a LDA seizure classifier that was trained using human CHB-MIT dataset (Goldberger et al., 2000). The LDA seizure classifier had accuracy 92.68%, sensitivity 76.88%, and specificity 93% that was comparable to the published prior work using the CHB-MIT dataset (Shoeb and Guttag, 2010). Then, the trained LDA seizure classifier was used to label the seizure data segments (= 3.4 sec) in the perinatal ovine model EEG data and the human EEG data. ARX parameters from the EEG-fNIRS seizure-free data segments (in 60 sec windows) from perinatal ovine model achieved accuracy of 95.30%, sensitivity of 91.95%, and specificity of 96.75%. The perinatal ovine model trained hierarchical classifier was applied to the human data where it labelled the six severe HIE cases and four severe HIE cases with sepsis as "hypoxia" and the four moderate HIE cases as the "control". Therefore, we showed the technical feasibility of our two-level hierarchical classifier in differentiating severe HIE from the moderate HIE which is feasible for hardware implementation (Hardware Implementation of Autoregressive Model Estimation Using Burg's Method for Low-Energy Spectral Analysis, n.d.).

Prolonged hypoxic event in the ovine model led to substantial seizure activity when the neonates are inherently susceptible to seizures with many more excitatory synapses than inhibitory synapses. So, the seizure data segments (= 3.4 sec) were removed using LDA classifier, trained with the CHB-MIT dataset (Goldberger et al., 2000), before second level HIE classification. Here, LDA classifier used only EEG data for the classification of the seizure data segments since manually labelled CHB-MIT dataset did not provide simultaneous fNIRS data. Then, our second level SVM classifier using ARX

 doi:10.20944/preprints202305.2080.v1



parameters from the EEG-fNIRS seizure-free data segments (in 60 sec windows) performed better in terms of sensitivity and specificity than the SVM classifier using AR parameters from the EEG seizure-free data segments – see Table 3 and 4. Indeed, tissue oxygenation and hemodynamics can provide additional information (Mitra et al., 2020) including seizure effects on the neurovascular tissue (Farrell et al., 2016), as shown by our perinatal ovine model data (see bottom panel of Figure 4), that may guide the hemodynamic care (Pang et al., 2020) especially in the severe HIE cases with seizure load that's time-critical (Pavel et al., 2022). Under oxygen starvation, an extracellular increase in the gamma-aminobutyric acid (GABA), the most common inhibitory neurotransmitter, can help in the metabolic suppression (Kolesnikova, 2023) that has a correlate in the hemodynamics and neurovascular coupling (Lim et al., 2021) – the excitation/inhibition (E/I) ratio can be estimated with EEG-fNIRS (Dagar et al., 2016). Importantly, the neurodevelopmental circuits in neonates under HIE insults may maladaptively coordinate their excitatory and inhibitory inputs to establish E/I ratio (He and Cline, 2019) where neuroenergetics may play a crucial role (Dutta et al., 2020). For example, hypoglycaemia may reduce GABA levels due to ATP depletion in hypoxia state (Madl and Royer, 2000). Then, the effects on the cerebellum (Pae et al., 2011) may be underestimated (Annink et al., 2021) that needs future development of whole head fNIRS technology (Rocco et al., 2021),(Singh et al., 2021) for neonates as the thin skin and skull allow deep penetration of the NIR light. Cerebellar Purkinje fibres are sensitive to hypoxic injury and can show damage even in the mild cases of HIE (White et al., 2013). Indeed, HIE accounts for chronic cerebellar deficits, including schizophrenia and other nonaffective psychoses (Zornberg et al., 2000), which create an economic burden so low-cost technological innovations are crucial (Ram et al., 2020).

Our perinatal ovine hypoxia model benefited from previous studies on animal models of hypoxia-ischemia for mechanistic understanding of the SVM classifier results. In the study by Bjorkman et al. (Björkman et al., 2010), the ictal activity was subclassified into two subgroups, clinical and subclinical. Clinical seizures had some visual effect on movement, limb jerks, or mouth quivering, while subclinical seizures can only be detected by abnormalities in the EEG with absence of movement. In this study on 28 piglets with 77 percent ictal activity, the background EEG showed lower amplitude compared to that of the nonseizure ischemic state. This supports our SVM classifier approach where we analysed the background EEG after removing seizure data segments (using the first level LDA seizure classifier). Here, a lower amplitude background EEG activity can be marker of an increased neurological damage where the importance of a lower amplitude background EEG activity was shown by histological analysis after euthanasia (Björkman et al., 2010). Then, fast oscillations (>40Hz) in neonatal EEG are rare and high gamma frequencies (Takeuchi et al., 2021) evaded our first level LDA classifier. More advanced seizure detection methods are available to identify fast oscillations (>40Hz)(Takeuchi et al., 2021), e.g., in previous publications (Puspita et al., 2017),(Zacharaki et al., 2016) researchers have used backpropagation neural networks (Puspita et al., 2017) with an input layer of 9 neurons, a hidden layer of 2 to 3 neurons, and an output layer containing one neuron. The input layer was trained on statistical measures of the ictal waveform itself. They used this classifier to identify the differences between EEG activity and did so with a 93.75% accuracy. Another group (Zacharaki et al., 2016) attempted to identify all ictal activity with one classifier by dividing peaks that are separated enough to be considered seizures, that is, at least 100ms. Then, they analysed the portions of the wave before and after the peak with the amplitude difference and the duration of the wave. These parameters of each half-wave were used to train an SVM with a high sensitivity of 97%. Many advanced machine learning algorithms are under development; however, their clinical utility beyond conventional EEG needs further investigation especially in a limited resource settings (Pavel et al., 2020).

In the current study, we showed the importance of EMA of the NVC system from the seizure-free background EEG and fNIRS data that provided insights. Here, stabilisation diagrams with and without stable poles were found for the different cases of severe HIE, severe HIE with sepsis, and moderate HIE. However, the clinical and physiological significance of the dip around 1 Hz as well as a stable pole mainly in the frequency between 0.5Hz and 1Hz in the four severe HIE human perinatal cases with sepsis (see Figure 5) need a larger clinical study with another control group with depressed

neonates without HIE. Here, changes in the NVC due to HIE has been demonstrated by previous works by the Chalak group (Chalak et al., 2017),(Das et al., 2021); however, our systems analysis using EMA may provide further insights into the neurovascular (and neurometabolic) dynamics. Neurovascular (and neurometabolic) dynamics is also relevant in the adult acute brain injury cases where normalization of neurovascular coupling may herald recovery of consciousness (Othman et al., 2020). Here, the effects of seizure activity on the coupling dynamics of the neural activity (measured with EEG) with the cerebral metabolism, oxygen delivery and blood volume may be crucial to guide medication (Farrell et al., 2016, 2017, n.d.), especially by leveraging optical monitoring in neonates (Howard et al., 2022). Other relevant chromophores, cytochrome c oxidase (CCO) and water, can also be investigated with optical monitoring in the neonates (Howard et al., 2022), which was developed in another study by adding four different wavelengths (780nm, 810nm, 820nm, 840nm) to low-cost EEG-fNIRS sensor (https://neuromodec.org/nyc-neuromodulation-online-2020/P18.html)(Karanth et al., 2022). In that case series (Karanth et al., 2022), we found that the neurometabolic coupling was specifically affected in the HIE with sepsis which may be related to the differences in the stabilization diagrams (see Figure 5) between the six severe HIE human perinatal cases and the four severe HIE human perinatal cases with sepsis. Howard et al. (Howard et al., 2022) highlighted the importance of the estimation of the oxidation state of the CCO (oxCCO) concentration changes in HIE. Here, CCO is essential to generate ATP efficiently during aerobic respiration so the effects of seizure activity on the background EEG and oxCCO will be important to study its metabolic effects (Howard et al., 2022). Then, Howard et al. (Howard et al., 2022) reviewed literature that showed pre-ictal changes in the cerebral hemodynamics that aligns with our perinatal ovine data (Hagan, 2018) – see Figure 4. Figure 4 shows a small increase in the preictal carotid artery flow that was also detected with fNIRS and may improve the latency (or even predict (Rosas-Romero et al., 2019)) of ictal period classification when fNIRS is added to the EEG monitoring of seizure activity. Also, the accuracy of the ictal period classification may be improved with multimodal EEG-fNIRS data due to primarily biphasic response of oxyhemoglobin and deoxyhemoglobin concentration changes (Howard et al., 2022). Nevertheless, the hemodynamic responses to seizures are not uniform across literature (Howard et al., 2022) and the individual differences in the neurovascular and neurometabolic coupling may subserve the effects of seizures on the brain tissue (Farrell et al., 2017). For example, any progressive decrease in oxCCO baseline with sequential seizures (Mitra et al., 2016) needs future investigation vis-à-vis clinical outcomes including exacerbation of epileptogenesis following HIE (Mitra et al., 2019).

Hypoglycemia is a common metabolic problems of the malnourished newborn due to working mothers in lower income countries (Aliefendioğlu et al., 2018), which can also disturb brain metabolism in HIE. A multiscale model will be needed for the mechanistic understanding of the hypoglycemia effects on the outcome from HIE and sequential seizure events. Then, sepsis is characterized by systemic changes in the metabolism (Preau et al., 2021) that can further disturb brain metabolism in HIE where optical monitoring can provide insights (Howard et al., 2022). Prior work by Jolivet et al. (Jolivet et al., 2015) provided a detailed neurometabolic model that captured the concentration of lactate in the neuronal, astrocytic and extracellular compartments that were coupled as modulatory feedback (Bozzo et al., 2013; Mosienko et al., 2015) with the voltage of the neuronal membrane. Such mechanistic investigation is crucial since oxygen and glucose deprivation can lead to an increase in the extracellular concentrations of excitatory amino acid neurotransmitters (Martin et al., 1994) leading to an E-I imbalance in the brain tissue (at the level of neuronal circuits) (Dutta et al., 2020). Then, neuronal circuit may try to self-organize towards E-I balance (Sukenik et al., 2021) via changes in the connectivity that can be dysfunctional when there is a genetic risk (Cannon et al., 2002),(Huang et al., 2021). Also, hypoxia-ischemia induced gene transcription effects are possible (Dupré et al., 2020). Previous work on patient-derived cerebral organoids has revealed gene expression patterns suggesting dysregulation of mitochondrial function (Kathuria et al., 2020) that can lead to long-term deficits in synaptic E-I balance in the susceptible individuals. Such gene-environment interactions can be investigated mechanistically using a subject-specific brain organoid model from human-induced pluripotent stem cells (iPSC) to test optical theranostics (Karanth et al.,

2022). Then, oxygen glucose deprivation can be easily implemented in an in-vitro subject-specific brain organoid model (Karanth et al., 2022) for mechanistic studies. Notably, our in-vitro subject-specific brain organoid study (https://neuromodec.org/nyc-neuromodulation-online-2020/P18.html)(Karanth et al., 2022) showed an increase in the CCO activity and pH in the organoid tissue and a decrease in the electrophysiological spectral exponent (related to E-I balance (Lombardi et al., 2017)) following photobiomodulation. These preliminary results are important for future works on non-pharmacological therapeutics since histogenous hypoxia and acid retention is closely related to glucose metabolism (Huang et al., 2021) that may be photobiomodulated (https://neuromodec.org/nyc-neuromodulation-online-2020/P18.html)(Karanth et al., 2022) – needs future investigation. In our phase zero studies (Dutta et al., 2020), the brain organoid platform (Karanth et al., 2022) can use a dual polymer sensor in the Matrigel matrix to provide real-time glucose and oxygen monitoring (Zhang et al., 2013) during mitochondrial photobiomodulation to capture the neurometabolic dose/response relationship for individualized delivery (Arora and Dutta, 2022). However, our brain organoid (Karanth et al., 2022) cannot currently model neurovascular coupling which may be feasible with vascularized organoids (Zhao et al., 2021).

In conclusion, the current study showed the feasibility of multimodal EEG-fNIRS data acquisition and EMA approach for the systems analysis of NVC that may provide biomarker of the sepsis effects on the neurovascular brain tissue in human HIE. Here, the EMA approach to the NVC dynamics using EEG-fNIRS data is novel in our knowledge; however, the systems analysis may need to be extended beyond the neurovascular bundle (Chalak and Zhang, 2017) to include non-invasive measurement of the blood pressure and cardiac output (e.g., electrocardiogram of the heart rate) in the human studies (see Figure 1 and the published results from the perinatal asphyxiated lamb model experiments (Vali et al., 2018)). Then, cerebral blood flow (CBF) is regulated by cerebral autoregulation, cerebral vasoreactivity, and neurometabolic coupling (Diehl et al., 1995),(Honma et al., 1987) that can be monitored using cerebral near infrared spectroscopy (Mitra et al., 2020). Also, seizure induced autonomic dysfunction is possible (Ferlini et al., 2021) that requires systems analysis beyond EEG and fNIRS with the inclusion of simultaneous blood pressure and cardiac monitoring. Here, the effect of preictal increase in the CBF during a severe metabolic deficit in HIE (e.g., slowing of background EEG) may be physiologically important (Björkman et al., 2010),(Schwartz et al., 2011),(Vinette et al., 2016),(Naftulin et al., 2018) – see Figure S4 from the perinatal asphyxiated lamb model experiments in the Supplementary Materials. So, a unified theory of seizure-induced brain state abnormalities including the effects of sepsis, which may share a common point of origin with hypoperfusion/hypoxia (Farrell et al., 2017), needs future investigation for the development of a robust biomarker amenable to optical brain tissue monitoring in the neonates (Howard et al., 2022).

**Supplementary Materials:** The following supporting information can be downloaded at the website of this paper posted on Preprints.org.

**Authors' Contributions:** AnD developed the multimodal neuroimaging and systems analysis of the neurovascular coupling concept, supervised BH and RM on hardware development, computational modelling, and supporting human and animal studies. AbD was the principal investigator for the Bill and Melinda Gates Foundation & IKP Knowledge Park, Department of Biotechnology (DBT), Government of India for human neonatal studies in India, while AnD was the principal investigator for the Global Health Equity Seed Funding, University at Buffalo, USA, for supporting the preclinical animal studies in the USA and the clinical human studies in India. JPS was the lead for the neonatal study in IMS & SUM Hospital, Bhubaneswar, India.

**Funding:** The study was funded by the Community for Global Health Equity Seed Funding, University of Buffalo, Department of Biotechnology (DBT), Government of India, the Bill and Melinda Gates Foundation & IKP Knowledge Park, India. Radhika Mujumdar was partially funded as an intern by the Community for Global Health Equity Seed Funding, University of Buffalo.

**Acknowledgments:** The authors thankfully acknowledge that the animal studies were conducted in the laboratory of Satyan Lakshminrusimha of the University of Buffalo, USA, and the human studies were conducted at IMS & SUM hospital, Bhubaneswar, India. We also thankfully acknowledge that the manuscript is partly based on the master's thesis by Brian Hagan (Hagan, 2018) with the committee consisting of Albert Titus, Praveen Chandrasekharan, and Jayasree Nair at the University at Buffalo, USA.

**Conflict of Interest:** The authors declare that the research was conducted in the absence of commercial or financial relationships that could be construed as a potential conflict of interest.

## Reference


Ahmed, R., Temko, A., Marnane, W., Lightbody, G., and Boylan, G. (2016). Grading hypoxic-ischemic encephalopathy severity in neonatal EEG using GMM supervectors and the support vector machine. *Clin Neurophysiol* 127, 297–309. doi: 10.1016/j.clinph.2015.05.024.

Al-Fahoum, A. S., and Al-Fraihat, A. A. (2014). Methods of EEG signal features extraction using linear analysis in frequency and time-frequency domains. *ISRN Neurosci* 2014, 730218. doi: 10.1155/2014/730218.

Aliefendioğlu, D., Çoban, A., Hatipoğlu, N., Ecevit, A., Arısoy, A. E., Yeşiltepe, G., et al. (2018). Management of hypoglycemia in newborn: Turkish Neonatal and Pediatric Endocrinology and Diabetes Societies consensus report. *Turk Pediatri Ars* 53, S224–S233. doi: 10.5152/TurkPediatriArs.2018.01820.

Annink, K. V., Meerts, L., van der Aa, N. E., Alderliesten, T., Nikkels, P. G. J., Nijboer, C. H. A., et al. (2021). Cerebellar injury in term neonates with hypoxic-ischemic encephalopathy is underestimated. *Pediatr Res* 89, 1171–1178. doi: 10.1038/s41390-020-01173-z.

Arora, Y., and Dutta, A. (2022). Human-in-the-Loop Optimization of Transcranial Electrical Stimulation at the Point of Care: A Computational Perspective. *Brain Sciences* 12, 1294. doi: 10.3390/brainsci12101294.

Björkman, S. T., Miller, S. M., Rose, S. E., Burke, C., and Colditz, P. B. (2010). Seizures are associated with brain injury severity in a neonatal model of hypoxia-ischemia. *Neuroscience* 166, 157–167. doi: 10.1016/j.neuroscience.2009.11.067.

Bozzo, L., Puyal, J., and Chatton, J.-Y. (2013). Lactate Modulates the Activity of Primary Cortical Neurons through a Receptor-Mediated Pathway. *PLOS ONE* 8, e71721. doi: 10.1371/journal.pone.0071721.

Bryce, J., Victora, C. G., Habicht, J.-P., Black, R. E., Scherpbier, R. W., and MCE-IMCI Technical Advisors (2005). Programmatic pathways to child survival: results of a multi-country evaluation of Integrated Management of Childhood Illness. *Health Policy Plan* 20 Suppl 1, i5–i17. doi: 10.1093/heapol/czi055.

Cannon, T. D., van Erp, T. G. M., Rosso, I. M., Huttunen, M., Lönnqvist, J., Pirkola, T., et al. (2002). Fetal hypoxia and structural brain abnormalities in schizophrenic patients, their siblings, and controls. *Arch Gen Psychiatry* 59, 35–41. doi: 10.1001/archpsyc.59.1.35.

Chalak, L. F., Tian, F., Adams-Huet, B., Vasil, D., Laptook, A., Tarumi, T., et al. (2017). Novel Wavelet Real Time Analysis of Neurovascular Coupling in Neonatal Encephalopathy. *Scientific Reports* 7, 45958. doi: 10.1038/srep45958.

Chalak, L. F., and Zhang, R. (2017). New Wavelet Neurovascular Bundle for Bedside Evaluation of Cerebral Autoregulation and Neurovascular Coupling in Newborns with Hypoxic Ischemic Encephalopathy. *Dev Neurosci* 39, 89–96. doi: 10.1159/000457833.

Choi, D. W. (1990). Cerebral hypoxia: some new approaches and unanswered questions. *J Neurosci* 10, 2493–2501.

Dagar, S., Chowdhury, S. R., Bapi, R. S., Dutta, A., and Roy, D. (2016). Near-Infrared Spectroscopy – Electroencephalography-Based Brain-State-Dependent Electrotherapy: A Computational Approach Based on Excitation–Inhibition Balance Hypothesis. *Front Neurol* 7. doi: 10.3389/fneur.2016.00123.

Das, Y., Leon, R. L., Liu, H., Kota, S., Liu, Y., Wang, X., et al. (2021). Wavelet-based neurovascular coupling can predict brain abnormalities in neonatal encephalopathy. *Neuroimage Clin* 32, 102856. doi: 10.1016/j.nicl.2021.102856.

Del Río, R., Ochoa, C., Alarcon, A., Arnáez, J., Blanco, D., and García-Alix, A. (2016). Amplitude Integrated Electroencephalogram as a Prognostic Tool in Neonates with Hypoxic-Ischemic Encephalopathy: A Systematic Review. *PLoS One* 11, e0165744. doi: 10.1371/journal.pone.0165744.

Diehl, R. R., Linden, D., Lücke, D., and Berlit, P. (1995). Phase relationship between cerebral blood flow velocity and blood pressure. A clinical test of autoregulation. *Stroke* 26, 1801–1804. doi: 10.1161/01.str.26.10.1801.

Dupré, N., Derambure, C., Le Dieu-Lugon, B., Hauchecorne, M., Detroussel, Y., Gonzalez, B. J., et al. (2020). Hypoxia-Ischemia Induced Age-Dependent Gene Transcription Effects at Two Development Stages in the Neonate Mouse Brain. *Frontiers in Molecular Neuroscience* 13. Available at: https://www.frontiersin.org/articles/10.3389/fnmol.2020.587815 [Accessed May 1, 2023].

Dutta, A., Karanth, S. S., Bhattacharya, M., Liput, M., Augustyniak, J., Cheung, M., et al. (2020). A proof of concept 'phase zero' study of neurodevelopment using brain organoid models with Vis/near-infrared spectroscopy and electrophysiology. *Scientific Reports* 10, 20987. doi: 10.1038/s41598-020-77929-8.

Faes, L., Pinna, G. D., Porta, A., Maestri, R., and Nollo, G. (2004). Surrogate data analysis for assessing the significance of the coherence function. *IEEE Transactions on Biomedical Engineering* 51, 1156–1166. doi: 10.1109/TBME.2004.827271.

Farrell, J. S., Colangeli, R., Wolff, M. D., Wall, A. K., Phillips, T. J., George, A., et al. (2017). Postictal hypoperfusion/hypoxia provides the foundation for a unified theory of seizure-induced brain abnormalities and behavioral dysfunction. *Epilepsia* 58, 1493–1501. doi: 10.1111/epi.13827.

Farrell, J. S., Gaxiola-Valdez, I., Wolff, M. D., David, L. S., Dika, H. I., Geeraert, B. L., et al. (2016). Postictal behavioural impairments are due to a severe prolonged hypoperfusion/hypoxia event that is COX-2 dependent. *eLife* 5, e19352. doi: 10.7554/eLife.19352.

Farrell, J. S., Gaxiola-Valdez, I., Wolff, M. D., David, L. S., Dika, H. I., Geeraert, B. L., et al. (n.d.). Postictal behavioural impairments are due to a severe prolonged hypoperfusion/hypoxia event that is COX-2 dependent. *eLife* 5, e19352. doi: 10.7554/eLife.19352.

Ferlini, L., Su, F., Creteur, J., Taccone, F. S., and Gaspard, N. (2021). Cerebral and systemic hemodynamic effect of recurring seizures. *Sci Rep* 11, 22209. doi: 10.1038/s41598-021-01704-6.

Goel, V., Brambrink, A. M., Baykal, A., Koehler, R. C., Hanley, D. F., and Thakor, N. V. (1996). Dominant frequency analysis of EEG reveals brain's response during injury and recovery. *IEEE Transactions on Biomedical Engineering* 43, 1083–1092. doi: 10.1109/10.541250.

Goldberger, A. L., Amaral, L. A., Glass, L., Hausdorff, J. M., Ivanov, P. C., Mark, R. G., et al. (2000). PhysioBank, PhysioToolkit, and PhysioNet: components of a new research resource for complex physiologic signals. *Circulation* 101, E215-220. doi: 10.1161/01.cir.101.23.e215.

Greene, B. R., Faul, S., Marnane, W. P., Lightbody, G., Korotchikova, I., and Boylan, G. B. (2008). A comparison of quantitative EEG features for neonatal seizure detection. *Clin Neurophysiol* 119, 1248–1261. doi: 10.1016/j.clinph.2008.02.001.

Hagan, B. (2018). Classification of Electroencephalogram in Ovine Model of Perinatal Hypoxia by Movement of the Autoregressive Model Parameters. Available at: http://ubir.buffalo.edu/xmlui/handle/10477/78010 [Accessed March 5, 2019].

Hardware Implementation of Autoregressive Model Estimation Using Burg's Method for Low-Energy Spectral Analysis (n.d.). Available at: https://ieeexplore.ieee.org/document/8598315 [Accessed April 30, 2023].

He, H., and Cline, H. T. (2019). What Is Excitation/Inhibition and How Is It Regulated? A Case of the Elephant and the Wisemen. *J Exp Neurosci* 13, 1179069519859371. doi: 10.1177/1179069519859371.

Honma, Y., Nagao, S., Tsutsui, T., Sunami, N., Momma, F., Kuyama, H., et al. (1987). [Interaction between neurogenic and metabolic factors upon deterioration in cerebrovascular tonus--experimental study on the etiology of cerebral vasoparesis]. *No To Shinkei* 39, 1061–1068.

Howard, R., Li, R., Harvey-Jones, K., Verma, V., Lange, F., Boylan, G., et al. (2022). Optical Monitoring in Neonatal Seizures. *Cells* 11, 2602. doi: 10.3390/cells11162602.

Huang, X., Lu, Q.-L., Zhu, X.-M., Zeng, Y.-B., Liu, Y., and Hu, H.-Y. (2021). Histogenous Hypoxia and Acid Retention in Schizophrenia: Changes in Venous Blood Gas Analysis and SOD in Acute and Stable Schizophrenia Patients. *Front Psychiatry* 12, 792560. doi: 10.3389/fpsyt.2021.792560.

Huppert, T. J. (2016). Commentary on the statistical properties of noise and its implication on general linear models in functional near-infrared spectroscopy. *Neurophotonics* 3, 010401. doi: 10.1117/1.NPh.3.1.010401.

Jolivet, R., Coggan, J. S., Allaman, I., and Magistretti, P. J. (2015). Multi-timescale Modeling of Activity-Dependent Metabolic Coupling in the Neuron-Glia-Vasculature Ensemble. *PLOS Computational Biology* 11, e1004036. doi: 10.1371/journal.pcbi.1004036.

Jouny, C. C., and Bergey, G. K. (2012). Characterization of Early Partial Seizure Onset: Frequency, Complexity and Entropy. *Clin Neurophysiol* 123, 658–669. doi: 10.1016/j.clinph.2011.08.003.

Karanth, S. S., Mujumdar, R., Sahoo, J. P., Das, A., Stachowiak, M. K., and Dutta, A. (2022). Human Brain Organoid Platform for Neuroengineering Optical Theranostics in Neonatal Sepsis. in *Converging Clinical and Engineering Research on Neurorehabilitation IV* Biosystems & Biorobotics., eds. D. Torricelli, M. Akay, and J. L. Pons (Cham: Springer International Publishing), 753–757. doi: 10.1007/978-3-030-70316-5_120.

Kathuria, A., Lopez-Lengowski, K., Jagtap, S. S., McPhie, D., Perlis, R. H., Cohen, B. M., et al. (2020). Transcriptomic Landscape and Functional Characterization of Induced Pluripotent Stem Cell–Derived Cerebral Organoids in Schizophrenia. *JAMA Psychiatry* 77, 745–754. doi: 10.1001/jamapsychiatry.2020.0196.

Kolesnikova, E. E. (2023). GABAergic Mechanisms of Brain Tolerance to Hypoxia in Lower Vertebrates. *J Evol Biochem Phys* 59, 522–541. doi: 10.1134/S0022093023020199.

Kyng, K. J., Skajaa, T., Kerrn-Jespersen, S., Andreassen, C. S., Bennedsgaard, K., and Henriksen, T. B. (2015). A Piglet Model of Neonatal Hypoxic-Ischemic Encephalopathy. *J Vis Exp*, e52454. doi: 10.3791/52454.

Laerhoven, H. van, Haan, T. R. de, Offringa, M., Post, B., and Lee, J. H. van der (2012). Prognostic Tests in Term Neonates With Hypoxic-Ischemic Encephalopathy: A Systematic Review. *Pediatrics*, peds.2012-1297. doi: 10.1542/peds.2012-1297.

Lawn, J. E., Cousens, S., Zupan, J., and Lancet Neonatal Survival Steering Team (2005). 4 million neonatal deaths: when? Where? Why? *Lancet* 365, 891–900. doi: 10.1016/S0140-6736(05)71048-5.

Lim, H.-K., You, N., Bae, S., Kang, B.-M., Shon, Y.-M., Kim, S.-G., et al. (2021). Differential contribution of excitatory and inhibitory neurons in shaping neurovascular coupling in different epileptic neural states. *J Cereb Blood Flow Metab* 41, 1145–1161. doi: 10.1177/0271678X20934071.

Lombardi, F., Herrmann, H. J., and de Arcangelis, L. (2017). Balance of excitation and inhibition determines 1/f power spectrum in neuronal networks. *Chaos* 27, 047402. doi: 10.1063/1.4979043.

Louis, E. K. S., Frey, L. C., Britton, J. W., Frey, L. C., Hopp, J. L., Korb, P., et al. (2016). "The Developmental EEG: Premature, Neonatal, Infant, and Children," in *Electroencephalography (EEG): An Introductory Text and Atlas of Normal and Abnormal Findings in Adults, Children, and Infants [Internet]* (American Epilepsy Society). Available at: https://www.ncbi.nlm.nih.gov/books/NBK390356/ [Accessed April 30, 2023].

Madl, J. E., and Royer, S. M. (2000). Glutamate dependence of GABA levels in neurons of hypoxic and hypoglycemic rat hippocampal slices. *Neuroscience* 96, 657–664. doi: 10.1016/s0306-4522(99)00548-5.

Martin, R. L., Lloyd, H. G. E., and Cowan, A. I. (1994). The early events of oxygen and glucose deprivation: setting the scene for neuronal death? *Trends in Neurosciences* 17, 251–257. doi: 10.1016/0166-2236(94)90008-6.

Mitra, S., Bale, G., Highton, D., Gunny, R., Uria-Avellanal, C., Bainbridge, A., et al. (2019). Pressure passivity of cerebral mitochondrial metabolism is associated with poor outcome following perinatal hypoxic ischemic brain injury. *J Cereb Blood Flow Metab* 39, 118–130. doi: 10.1177/0271678X17733639.

Mitra, S., Bale, G., Mathieson, S., Uria-Avellanal, C., Meek, J., Tachtsidis, I., et al. (2016). Changes in Cerebral Oxidative Metabolism during Neonatal Seizures Following Hypoxic–Ischemic Brain Injury. *Front Pediatr* 4. doi: 10.3389/fped.2016.00083.

Mitra, S., Bale, G., Meek, J., Tachtsidis, I., and Robertson, N. J. (2020). Cerebral Near Infrared Spectroscopy Monitoring in Term Infants With Hypoxic Ischemic Encephalopathy—A Systematic Review. *Front Neurol* 11, 393. doi: 10.3389/fneur.2020.00393.

Mosienko, V., Teschemacher, A. G., and Kasparov, S. (2015). Is L-lactate a novel signaling molecule in the brain? *J. Cereb. Blood Flow Metab.* 35, 1069–1075. doi: 10.1038/jcbfm.2015.77.

Mrelashvili, A., Russ, J. B., Ferriero, D. M., and Wusthoff, C. J. (2020). The Sarnat Score for Neonatal Encephalopathy: Looking Back and Moving Forward. *Pediatr Res* 88, 824–825. doi: 10.1038/s41390-020-01143-5.

Naftulin, J. S., Ahmed, O. J., Piantoni, G., Eichenlaub, J.-B., Martinet, L.-E., Kramer, M. A., et al. (2018). Ictal and preictal power changes outside of the seizure focus correlate with seizure generalization. *Epilepsia* 59, 1398–1409. doi: 10.1111/epi.14449.

Othman, M. H., Bhattacharya, M., Møller, K., Kjeldsen, S., Grand, J., Kjaergaard, J., et al. (2020). Resting-State NIRS-EEG in Unresponsive Patients with Acute Brain Injury: A Proof-of-Concept Study. *Neurocrit Care*. doi: 10.1007/s12028-020-00971-x.

Pae, E.-K., Yoon, A. J., Ahuja, B., Lau, G. W., Nguyen, D. D., Kim, Y., et al. (2011). Perinatal intermittent hypoxia alters γ-aminobutyric acid: a receptor levels in rat cerebellum. *Int J Dev Neurosci* 29, 819–826. doi: 10.1016/j.ijdevneu.2011.09.003.

Pang, R., Mintoft, A., Crowley, R., Sellwood, M., Mitra, S., and Robertson, N. J. (2020). Optimizing hemodynamic care in neonatal encephalopathy. *Seminars in Fetal and Neonatal Medicine* 25, 101139. doi: 10.1016/j.siny.2020.101139.

Pavel, A. M., Rennie, J. M., de Vries, L. S., Blennow, M., Foran, A., Shah, D. K., et al. (2020). A machine-learning algorithm for neonatal seizure recognition: a multicentre, randomised, controlled trial. *The Lancet Child & Adolescent Health* 4, 740–749. doi: 10.1016/S2352-4642(20)30239-X.

Pavel, A. M., Rennie, J. M., Vries, L. S. de, Blennow, M., Foran, A., Shah, D. K., et al. (2022). Neonatal Seizure Management: Is the Timing of Treatment Critical? *The Journal of Pediatrics* 243, 61-68.e2. doi: 10.1016/j.jpeds.2021.09.058.

Preau, S., Vodovar, D., Jung, B., Lancel, S., Zafrani, L., Flatres, A., et al. (2021). Energetic dysfunction in sepsis: a narrative review. *Annals of Intensive Care* 11, 104. doi: 10.1186/s13613-021-00893-7.

Puspita, J. W., Soemarno, G., Jaya, A. I., and Soewono, E. (2017). Interictal Epileptiform Discharges (IEDs) classification in EEG data of epilepsy patients. *J. Phys.: Conf. Ser.* 943, 012030. doi: 10.1088/1742-6596/943/1/012030.

Ram, P. K., Berkelhamer, S. K., and Dutta, A. (2020). "Low-Tech Innovations to Prevent Neonatal Mortality: Perspectives from Public Health, Neonatology, and Biomedical Engineering," in *Transforming Global Health: Interdisciplinary Challenges, Perspectives, and Strategies*, eds. K. H. Smith and P. K. Ram (Cham: Springer International Publishing), 113–126. doi: 10.1007/978-3-030-32112-3_8.

Rocco, G., Lebrun, J., Meste, O., and Magnie-Mauro, M.-N. (2021). A Chiral fNIRS Spotlight on Cerebellar Activation in a Finger Tapping Task. *Annu Int Conf IEEE Eng Med Biol Soc* 2021, 1018–1021. doi: 10.1109/EMBC46164.2021.9629565.

Rosas-Romero, R., Guevara, E., Peng, K., Nguyen, D. K., Lesage, F., Pouliot, P., et al. (2019). Prediction of epileptic seizures with convolutional neural networks and functional near-infrared spectroscopy signals. *Computers in Biology and Medicine* 111, 103355. doi: 10.1016/j.compbiomed.2019.103355.

Santosa, H., Zhai, X., Fishburn, F., and Huppert, T. (2018). The NIRS Brain AnalyzIR Toolbox. *Algorithms* 11, 73. doi: 10.3390/a11050073.

Sarnat, H. B., and Sarnat, M. S. (1976). Neonatal encephalopathy following fetal distress. A clinical and electroencephalographic study. *Arch Neurol* 33, 696–705. doi: 10.1001/archneur.1976.00500100030012.

Schwartz, T. H., Hong, S.-B., Bagshaw, A. P., Chauvel, P., and Bénar, C.-G. (2011). Preictal changes in cerebral haemodynamics: Review of findings and insights from intracerebral EEG. *Epilepsy Research* 97, 252–266. doi: 10.1016/j.eplepsyres.2011.07.013.

Shoeb, A., and Guttag, J. (2010). Application of machine learning to epileptic seizure detection. in *Proceedings of the 27th International Conference on International Conference on Machine Learning* ICML'10. (Madison, WI, USA: Omnipress), 975–982.

Singh, S. M., Kumar, K. N., Walia, P., Ranjan, S., Rezaee, Z., Lahiri, U., et al. (2021). Functional near-infrared spectroscopy (fNIRS) of posterolateral cerebellum and prefrontal cortex for fNIRS-driven cerebellar tES – a case report. *Brain Stimulation: Basic, Translational, and Clinical Research in Neuromodulation* 14, 1692. doi: 10.1016/j.brs.2021.10.333.

Sood, M., Besson, P., Muthalib, M., Jindal, U., Perrey, S., Dutta, A., et al. (2016). NIRS-EEG joint imaging during transcranial direct current stimulation: Online parameter estimation with an autoregressive model. *J. Neurosci. Methods* 274, 71–80. doi: 10.1016/j.jneumeth.2016.09.008.

Staba, R., and Worrell, G. (2014). What is the importance of abnormal "background" activity in seizure generation? *Adv Exp Med Biol* 813, 43–54. doi: 10.1007/978-94-017-8914-1_3.

Stevenson, N. J., Korotchikova, I., Temko, A., Lightbody, G., Marnane, W. P., and Boylan, G. B. (2013). An Automated System for Grading EEG Abnormality in Term Neonates with Hypoxic-Ischaemic Encephalopathy. *Ann Biomed Eng* 41, 775–785. doi: 10.1007/s10439-012-0710-5.

Sukenik, N., Vinogradov, O., Weinreb, E., Segal, M., Levina, A., and Moses, E. (2021). Neuronal circuits overcome imbalance in excitation and inhibition by adjusting connection numbers. *Proceedings of the National Academy of Sciences* 118, e2018459118. doi: 10.1073/pnas.2018459118.

Takeuchi, A., Inoue, T., Nakamura, M., Kageyama, M., Akiyama, T., and Kobayashi, K. (2021). Case Report: High-Gamma Oscillations on an Ictal Electroencephalogram in a Newborn Patient With Hypoxic–Ischemic Encephalopathy. *Front Pediatr* 9, 679771. doi: 10.3389/fped.2021.679771.

Toet, M., Hellstrom-Westas, L., Groenendaal, F., Eken, P., and de Vries, L. S. (1999). Amplitude integrated EEG 3 and 6 hours after birth in full term neonates with hypoxic-ischaemic encephalopathy. *Arch Dis Child Fetal Neonatal Ed* 81, F19–F23.

Vali, P., Chandrasekharan, P., Rawat, M., Gugino, S., Koenigsknecht, C., Helman, J., et al. (2017). Hemodynamics and gas exchange during chest compressions in neonatal resuscitation. *PLOS ONE* 12, e0176478. doi: 10.1371/journal.pone.0176478.

Vali, P., Gugino, S., Koenigsknecht, C., Helman, J., Chandrasekharan, P., Rawat, M., et al. (2018). The Perinatal Asphyxiated Lamb Model: A Model for Newborn Resuscitation. *J Vis Exp*, 57553. doi: 10.3791/57553.

Vali, P., Sankaran, D., Rawat, M., Berkelhamer, S., and Lakshminrusimha, S. (2019). Epinephrine in Neonatal Resuscitation. *Children (Basel)* 6, E51. doi: 10.3390/children6040051.

Vinette, S. A., Premji, S., Beers, C. A., Gaxiola-Valdez, I., Pittman, D. J., Slone, E. G., et al. (2016). Pre-ictal BOLD alterations: Two cases of patients with focal epilepsy. *Epilepsy Research* 127, 207–220. doi: 10.1016/j.eplepsyres.2016.09.010.

von Luhmann, A., Wabnitz, H., Sander, T., and Muller, K.-R. (2017). M3BA: A Mobile, Modular, Multimodal Biosignal Acquisition Architecture for Miniaturized EEG-NIRS-Based Hybrid BCI and Monitoring. *IEEE Trans Biomed Eng* 64, 1199–1210. doi: 10.1109/TBME.2016.2594127.

Walsh, B. H., Murray, D. M., and Boylan, G. B. (2011). The use of conventional EEG for the assessment of hypoxic ischaemic encephalopathy in the newborn: a review. *Clin Neurophysiol* 122, 1284–1294. doi: 10.1016/j.clinph.2011.03.032.

White, M. L., Zhang, Y., Helvey, J. T., and Omojola, M. F. (2013). Anatomical patterns and correlated MRI findings of non-perinatal hypoxic–ischaemic encephalopathy. *Br J Radiol* 86, 20120464. doi: 10.1259/bjr.20120464.

Zacharaki, E. I., Mporas, I., Garganis, K., and Megalooikonomou, V. (2016). Spike pattern recognition by supervised classification in low dimensional embedding space. *Brain Inform* 3, 73–83. doi: 10.1007/s40708-016-0044-4.

Zhang, L., Su, F., Buizer, S., Lu, H., Gao, W., Tian, Y., et al. (2013). A dual sensor for real-time monitoring of glucose and oxygen. *Biomaterials* 34, 10.1016/j.biomaterials.2013.09.031. doi: 10.1016/j.biomaterials.2013.09.031.

Zhao, X., Xu, Z., Xiao, L., Shi, T., Xiao, H., Wang, Y., et al. (2021). Review on the Vascularization of Organoids and Organoids-on-a-Chip. *Frontiers in Bioengineering and Biotechnology* 9. Available at: https://www.frontiersin.org/articles/10.3389/fbioe.2021.637048 [Accessed May 1, 2023].

Zornberg, G. L., Buka, S. L., and Tsuang, M. T. (2000). Hypoxic-ischemia-related fetal/neonatal complications and risk of schizophrenia and other nonaffective psychoses: a 19-year longitudinal study. *Am J Psychiatry* 157, 196–202. doi: 10.1176/appi.ajp.157.2.196.